HAL
open science

Combined three-color LIF-PDA measurements and infrared thermography applied to the study of the spray impingement on a heated surface above the Leidenfrost regime

Alexandre Labergue, J.-D Pena-Carillo, Michel Gradeck, Fabrice Lemoine

To cite this version:

Alexandre Labergue, J.-D Pena-Carillo, Michel Gradeck, Fabrice Lemoine. Combined three-color LIF-PDA measurements and infrared thermography applied to the study of the spray impingement on a heated surface above the Leidenfrost regime. International Journal of Heat and Mass Transfer, 2017, 104, pp.1008-1021. 10.1016/j.ijheatmasstransfer.2016.07.029 . hal-01579535

HAL Id: hal-01579535

https://hal.science/hal-01579535v1

Submitted on 1 Sep 2017

HAL is a multi-disciplinary open access archive for the deposit and dissemination of scientific research documents, whether they are published or not. The documents may come from teaching and research institutions in France or abroad, or from public or private research centers.

L'archive ouverte pluridisciplinaire **HAL**, est destinée au dépôt et à la diffusion de documents scientifiques de niveau recherche, publiés ou non, émanant des établissements d'enseignement et de recherche français ou étrangers, des laboratoires publics ou privés.

Combined three-color LIF-PDA measurements and infrared thermography applied to the study of the spray impingement on a heated surface above the Leidenfrost regime

A. Labergue[1,2*], J-D. Pena-Carillo[1,2], M. Gradeck[1,2], F. Lemoine[1,2]
[1]LEMTA, UMR 7563, Université de Lorraine, Vandoeuvre-Lès-Nancy, 54518, France
[2] LEMTA, UMR 7563, CNRS, Vandoeuvre-Lès-Nancy, 54518, France

Abstract
This experimental study deals with the impingement of sprays on a heated wall in close to semi-industrial conditions. Therefore, an experimental set-up was specifically designed: high liquid mass flux (up to 8 kg/m²/s), large droplets (up to 300 µm) and high surface temperature widely above the Leidenfrost point (up to 800°C). The surface to be cooled is a 175 mm diameter nickel disk with 5 mm thickness heated by electromagnetic induction. The spraying devices consist in full cone sprays. Several studies, performed under these particular conditions, has allowed characterizing the heat flux removed by the spray by using techniques based on thermocouples or infrared thermography (IRT). However, to investigate more finely the heat transfer mechanism, it is necessary to measure the droplet temperature but, to date, no measurement for sprays are available in the literature. Therefore, the objective of the present work is to demonstrate the ability of the three-color Laser Induced Fluorescence (3cLIF) to meet this challenge. The combination of the 3cLIF with a Phase Doppler system allows also determining the droplet temperature per size class before and after impact. By adding the IRT measurements combined to an inverse heat conduction model, an energy balance is done in order to estimate the evaporated liquid mass. The influence of the normal Weber number on the liquid vaporization is investigated by using three sprays (Normal Weber numbers up to about 1500). Thereby, main results show that the droplets temperature after impact increases with the incident Weber number before to reach a plateau, attributed to the apparition of the splashing regime. The analysis of the energy balance shows that the mass of evaporated liquid decreases with the incident Weber number and the droplet heating. These first results are in well agreement with previous works conducted with single calibrated droplets, validating as the same time the use of combined 3cLIF-PDA measurements in the case of sprays.

Keywords: Phase Doppler measurements; infrared thermography; Laser induced fluorescence thermometry; spray impingement; spray cooling.

Nomenclature:

Nu	Nusselt number	(-)
Pr	Prandtl number	(-)
Re	Reynolds number	(-)
We	Weber number	(-)
K	Mundo number	(-)
Oh	Ohnesorge number	(-)
C_p	specific heat capacity	(J/Kg/K)
R	disk radius	(m)
R_f	fluorescence intensity ratio	(-)
e	disk thickness	(m)
h	heat transfer coefficient	(W/m²/K)
k	thermal conductivity	(W/m/K)

D	droplet diameter	(m)
I	laser intensity	(u.a.)
I_f	fluorescence intensity	(u.a.)
L	latent heat	(J/kg)
m	incident liquid mass surface density	(kg/m²)
m_e	evaporated liquid mass surface density	(kg/m²)
G	liquid mass flux	(kg/m²/s)
φ	heat flux density	(W/m²)
q	heat density or energy density	(J/m²)
w,v	normal and horizontal (radial) components of the droplet velocity	(m/s)
r, z	radial and vertical coordinate	(m)
T	Temperature	(°C)
t	Time	(s)
Δt_{Leid}	Duration of the Leidenfrost regime	(s)
V_c	3cLIF collection volume	(m³)

Greel symbols

β	thermal sensitivity of the fluorescence signal	(-)
λ	laser wavelength	(nm)
ρ	mass density	(kg/m³)
μ	dynamic viscosity	(Pa.s)
σ	surface tension	(kg/m²)

Subscripts

a	after impact
b	before impact
c	class diameter
d	droplet
i	spectral band of detection
l	property of liquid phase
m	averaged
n	normal to the surface
r	radius
$Leid$	Leidenfrost temperature
sat	liquid saturation properties
v	property of vapor phase
air	airflow
$film$	film condition
w	conditions at the disk surface
N	number
0	reference condition for 3cLIF measurements
10	mean diameter

1. Introduction

The use of water to cool hot surfaces is unavoidable when dissipation of high heat flux is required. The applications in the industry are numerous. Nuclear safety in case of accident due to the loss of coolant fluid or the thermal processing of alloys in steel industry require efficient cooling with high heat flux dissipation at high temperatures. Water cooling processes include pool boiling, impingement of liquid jets or sprays. Pool boiling and liquid jets provide high dissipation rates but they have generally failed to ensure uniform and controlled cooling. In [1], very high heat transfers in the stagnation zone of the jet have been observed, whereas the heat transfers are moderate in the

spreading zone. Comparatively, the use of sprays seems attractive for several reasons: a better spatial uniformity of the cooling can be achieved in association with a lower water consumption for the same heat transfer efficiency, thus leading to energy saving.

However, the use of sprays in industry processes is not yet sufficiently widespread. The reason is that the optimization of these processes suffers of a lack in understanding and knowledge of the mechanisms that occurs when droplets interact with a heated wall. Indeed, the governing parameters for the droplet interacting with a hot wall are numerous and strongly correlated. There are mainly the physical droplet properties (viscosity, mass density and surface tension), the impinging droplet normal velocity, the droplet diameter, the droplet temperature, the surface roughness and its temperature. A considerable attention has been paid throughout the last decades to understand the influence of these parameters. Generally, the authors focused their work either on the hydrodynamic of the impact or on the heat transfers. For instance, the influence of the physical liquid properties on the hydrodynamic of the impingement was investigated by Rioboo et al. [2] and Sikalo et al. [3] while Cossali et al. [4] studied the effect of surface properties like roughness. In order to characterize the heat transfers between the heated wall and the liquid, thermocouples embedded within the solid wall [5-10] or infra-red thermography combined with advanced modelling of heat transfers are the most common techniques encountered in the literature [11;12]. On the contrary, the characterization of the heat transfers from the point of view of the droplets (including liquid/gas phase and liquid/solid transfers) is generally poorly approached in the literature. The estimation of relative variation of the droplet sensible heat or the mass of evaporated liquid during the impact still remains unknown. Le Clercq [13] estimated the mass of evaporated single droplets by measuring the mass ratio between incoming and outgoing droplets with the help of a Phase Doppler system. Nevertheless, the analysis has encountered difficulties due to strong deformation of droplets after their impingement.

To evaluate properly the droplet sensible heat, the measurements of the droplet temperature is required. Obviously, only non-intrusive optical methods are able to measure this parameter. For instance, Global rainbow thermometry (GLM) is based on the dependency of the refractive index with the liquid temperature and was tested in the case of water sprays [14-16]. Spontaneous Raman scattering was also used to measure the droplet temperature [17-19]. Another family of methods are based on the Laser Induced Fluorescence (LIF). This technique is based on the thermal dependence of a fluorescent dye seeded in the liquid of interest at a very low concentration. In order to eliminate the influence of parameters that are hardly measurable, two fluorescence intensities are simultaneously measured on two distinct spectral bands, that have contrasted temperature sensitivities, in order to derive a ratio. The two-color LIF (2cLIF) was widely used in the case of single droplets in evaporation or combustion [20; 21]. In the case of droplet/wall interaction, an extension of the 2cLIF, the 2c Planar Laser Induced Fluorescence (2cPLIF), recently allowed measuring the droplet temperature of single calibrated droplets in the Leidenfrost regime [12]. The sensible heat gained during the impact was measured and, as a consequence, the mass of evaporated liquid was estimated by using an overall energy balance.

The present work aims to extend the 2cLIF technique in the case of sprays impinging on a heated wall. However, it was demonstrated that the direct application of the 2cLIF in the case of sprays was not straightforward [22; 23]. The extension of the 2cLIF for sprays technique gave rise to the three-color LIF (3cLIF). Besides, the 3cLIF was recently combined with Phase Doppler in order to obtain the droplet temperature per size class [24; 25].

Therefore, the main objective of the present study is to apply the combined 3cLIF-PDA measurements in a new field of interest. Indeed, according to our best knowledge, studies that deal with droplet temperature measurements in the particular case of a spray impinging onto a heated wall are not referenced in the literature. Furthermore, the present work aims to implement operating parameters that mimic industrial conditions: high liquid mass flux (up to 8 kg/m²/s), large droplets (up to 300 µm), high surface temperature (800°C) and large surface to be cooled (175 mm in diameter). A first study was achieved according to these experimental conditions: a PDA system was employed to measure

droplets properties before and after impact as well as an infrared thermometry (IRT) to evaluate the heat flux removed from the wall [26]. Here, the interest to combine the 3cLIF thermometry with a PDA device relies to the capability of measuring the droplet temperature per size classes before and after impact. Consequently, by including the information on the heat flux measured by IRT, an energy balance will be used in order to evaluate the evaporated liquid mass. The investigation of both droplet heating and vaporization is mainly focused on the influence of the incident normal Weber number. For that purpose, three sprays having different characteristic (cone angle, liquid mass flux distribution, droplet size and velocity distribution) are employed. Besides, the analysis is limited to the particular case of the Leidenfrost regime.

2. Spray facilities

Figure 1 depicts the experimental facilities designed for investigating the spray impingement. This set-up is based on those used in [26] with some significant modifications in order to implement properly the combined 3cLIF-PDA measurements. It consists mainly in a closed loop of the coolant fluid (*i.e.* water seeded with the essential fluorescent tracer for LIF thermometry), including a main tank (label (1)), a cylindrical experimental chamber (label (7)) where the surface to be cool takes place, a centrifugal pump (label (2)) to ensure the circulation of the fluid and a drain pipe (label (7')) connecting the tank and the experimental chamber. The surface is a disk made of nickel (label (5); radius $R = 87.5$ mm and thickness $e = 5$ mm) and the spraying devices consist in full cone sprays.

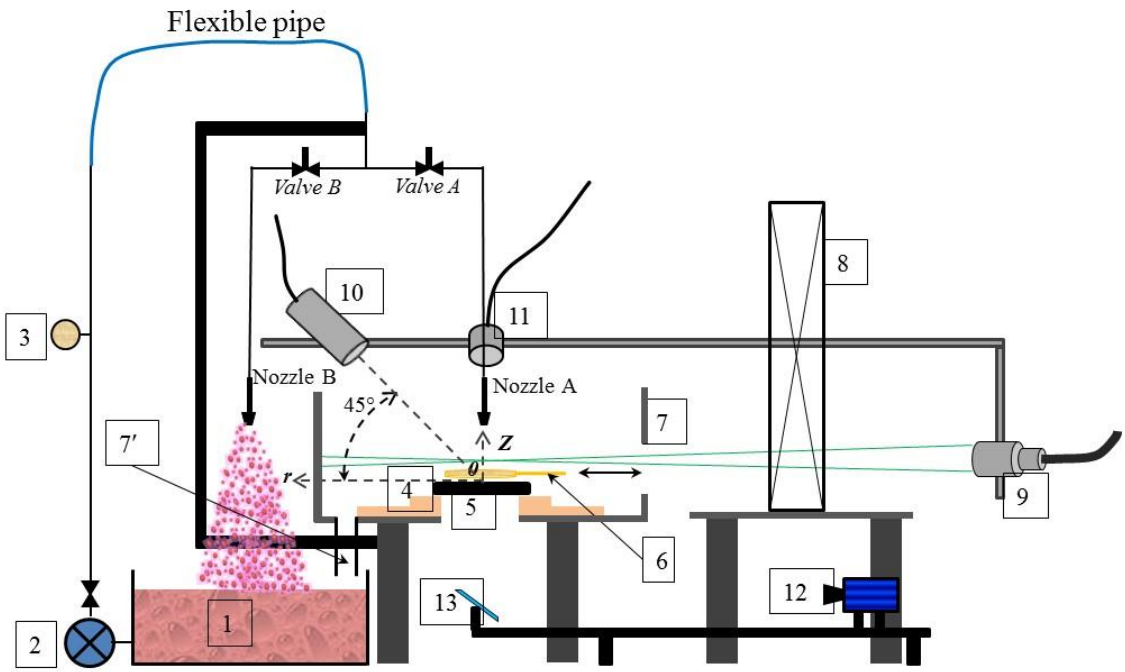

Figure 1: Experimental spray facilities and implementation of the optical measurement devices (combined LIF-PDA and IRT). Side view (*i.e. Z-r* plane) of the test rig. 1 – water tank; 2 – centrifugal pump; 3 – manometer; 4 – insulation part (quartz); 5 – nickel disk; 6 – retractable electromagnetic inductor; 7 – experimental chamber ; 7' – drain pipe; 8 – 3D traverse system; 9 – laser probe; 10 – PDA receiver; 11 – LIF collecting optics; 12 – IR camera; 13 – mirror.

Basically, an experiment is performed in two steps: the first one corresponds to the heating of the disk while the spray is turned-off and the second step corresponds to the quenching of the surface. In order to limit the establishment time of the spray flow (mainly due to the centrifugal pump start-

up time), a second similar spray is flowing directly on the tank during the first step. Two piloted electro-valves allow switching from one spray to the other one. The nickel disk is heated up by an electromagnetic induction system (power supply 12 kW; Five-Celes®). The disk is positioned on an insulating material (label (4)) and is centered just below the nozzle (A) along its main axis *Z*. The origin of both *r* and Z axis, *r* being the radial coordinate, is taken on the surface at the center of the disk.

The cylindrical chamber (450 mm in radius and 400 mm height) constitutes the main change compared to the set-up used in [26]. Its role is to prevent the splashing of water and protect the environment against the fluorescent tracer. Its radius value is taken large enough compared to the disk dimensions in order to not affect both the free flow spray and the impact. An aperture is provided for the laser path as well as a second one with a sliding window allowing the removal of the inductor during the cooling step. Three full cones spray (Lechler® nozzles) having different injection pressure and cone angles were used in order to vary the mass flux distribution impinging the surface as well as the incident normal Weber number distribution. Table 1 provides the main characteristics for the three sprays. The liquid mass flux *G* distribution along the radius of the disk has been already determined for these three sprays in absence of the disk in [26]. This parameter is plotted in Figure 2 at the three investigated radial position of the present study (see section 4. below). This parameter, as well as the mean normal Weber number before impact $\widehat{We_{nb}}$ (Figure 3), will be useful for the investigation of the heat and mass transfer which is detailed in section 4.3. The mean normal Weber number is deduced from PDA measurements and will be defined in section 3.4.

Table 1. Characteristics of the sprays considered in the present study.

Nozzle and spray number	Lechler® reference	Spray angle (°)	Flow rate (l/min)	Injection pressure (bar)	Nozzle-disk distance (mm)
1	460.643.17	45	6.7	7	250
2	460.683.17	45	6.7	3.7	250
3	460.684.17	60	6.7	3.7	160

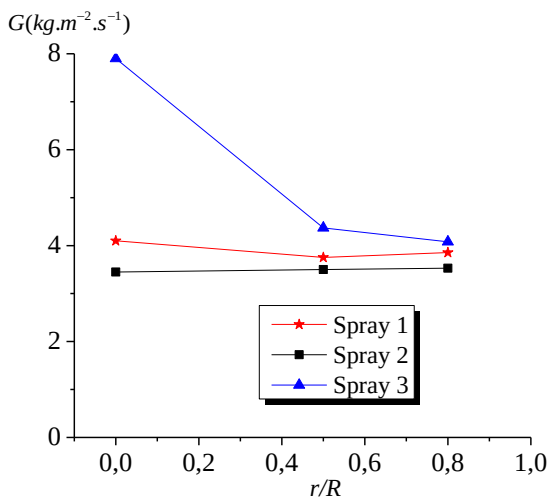

Figure 2. Liquid mass flux distribution for the three sprays plotted at three radial positions along the disk.

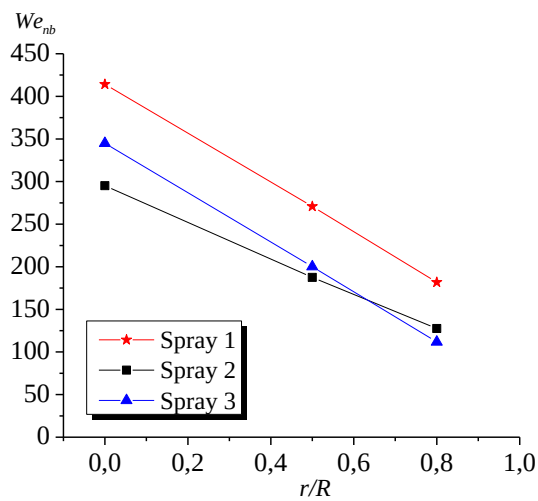

Figure 3. Mean normal Weber number distribution for the three sprays plotted at three radial positions along the disk.

3. Experimental diagnostics

This section is devoted to the presentation of the experimental diagnostics used in this study (3cLIF, PDA and IRT measurements). The basic principles are presented and a particular attention is paid in order to explain how these techniques are implemented and synchronized.

3.1 Principles of the three-color LIF thermometry

LIF thermometry is mainly based on 2cLIF. This technique was successfully validated in the case of single evaporating or combusting droplets [20; 21] and only the main features are summarized in this section. The liquid is preliminary seeded by a temperature sensitive fluorescent dye at a low molecular concentration. In the present work, the liquid is deionized water seeded with sulforhodamine B at a concentration of 5.10^{-6} mo.L^{-1}. The fluorescence is induced by the green line of an argon ion laser (λ = 514.5 nm). The fluorescence spectrum of sulforhodamine B is broadband and presents a temperature-dependent shape. Thus, the fluorescence intensity I_{fi} collected on a spectral band i can be expressed by [21]:

$$I_{fi}(T) \approx K_{opt,i} K_{spec,i} V_c I C e^{\frac{\beta_i}{T}} \quad (1)$$

where I is the local laser excitation intensity, C the fluorescent dye concentration, T the absolute temperature and V_c the collection volume of the fluorescence photons. This later is defined as the intersection of the illuminated part of the droplet volume in the field of view of the fluorescence collection optics. $K_{opt,i}$ and $K_{spec,i}$ are parameters influenced respectively by the optical layout and the spectral fluorescence properties of the fluorescent tracers. The parameter β_i corresponds to the temperature sensitivity of the fluorescence signal detected on the spectral band i. The parameters C, V_c and I are not constant when a droplet, potentially evaporating, moves in the laser excitation volume and therefore are unknown. These parameters can be removed by collecting simultaneously the fluorescence signal on two spectral bands, respectively I_{f1} and I_{f2}, and by calculating their ratio R_{f12}. Finally, a single reference R_{f120} measurement at a known temperature T_0 allows eliminating both constants $K_{opt,i}$ and $K_{spec,i}$. Then, a normalized ratio R_{f12}/R_{f120} depending only on temperature can be derived:

$$\frac{R_{f12}}{R_{f12o}} = \frac{I_{f1}}{I_{f2}} = e^{\beta_{12}\left(\frac{1}{T}-\frac{1}{T_0}\right)} \quad (2)$$

where $\beta_{12} = \beta_1 - \beta_2$.

In the present study, the selected spectral bands are: band 1 [535 nm; 545 nm] and band 2 [615 nm; 750 nm]. These bands allow obtaining a reasonable sensitivity of the fluorescence ratio on temperature. A calibration, conducted in a similar process as described in Depredurant et al., [27], leads to a temperature sensitivity of about 0.9%/K. In the work of Labergue et al., [21], a residual effect of the droplet diameter on the fluorescence ratio, not included in *eqn* (2), was highlighted. For instance, Figure 4, extracted from [21], depicts the evolutions of the normalized fluorescence ratio as function of the droplet diameter D in the particular case of single calibrated water droplets seeded with sulforhodamine B. Although these experiments were conducted under isothermal conditions, a significant increase of the fluorescence ratio is observed when decreasing the droplet diameter; otherwise the normalized fluorescence ratio tends to 1 for the largest droplet diameters. To account for the effect of the droplet size on the fluorescence ratio, an empirical function $g_{12}(D)$ was added in *eqn*. (2) [21]:

$$\frac{R_{f12}}{Rf_{12o}} = e^{\beta_{12}\left(\frac{1}{T}-\frac{1}{T_0}\right)} g_{12}(D) \quad (3)$$

To determine the unknown function $g_{12}(D)$, an empirical approach was undertaken [21]. The basic idea is to use a third spectral band to determine a second normalized fluorescence ratio:

$$\frac{R_{f32}}{R_{f32o}} = e^{\beta_{32}\left(\frac{1}{T}-\frac{1}{T_0}\right)} g_{32}(D) \tag{4}$$

The third spectral band is selected in order to minimize the temperature sensitivity of the ratio R_{f32} represented by the function $f_{32}(T)$. For the selected band, *i.e.* [555 nm; 575nm], the temperature sensitivity is on the order of 0.1 %/°C, which is much lower than $f_{12}(T)$. Similarly as for R_{f120}, a reference R_{f320} is taken at the same temperature T_0. Moreover, $g_{32}(D)$ is different from $g_{12}(D)$ and therefore the ratio R_{f32} has a different sensitivity on the droplet size compared to R_{f12}. As mentioned in Labergue et al., [23], an empirical relationship between both functions $g_{12}(D)$ and $g_{32}(D)$ can be determined experimentally by measuring the corresponding normalized fluorescence ratios for several droplet diameters under isothermal conditions. As a result, a monotonous evolution can be found, which can be easily interpolated by a second order polynomial:

$$g_{12} = \mathrm{a}{g_{32}}^2 + b g_{32} + c \tag{5}$$

This procedure is assumed available whatever the droplet diameter value and it will be seen in section 3.4 how it can be extended in the case of sprays. Finally, combining *eqn.* (3), (4) and (5) allows determining a relation between both fluorescence ratios (R_{f12} and R_{f32}) depending only on the temperature:

$$\frac{R_{f12}}{R_{f12o}} e^{\beta_{12}\left(\frac{1}{\mathrm{T}}-\frac{1}{\mathrm{T}_0}\right)} = a\left[e^{\beta_{32}\left(\frac{1}{\mathrm{T}_0}-\frac{1}{\mathrm{T}}\right)} \frac{R_{f32}}{R_{f32o}}\right]^2 + b\left[e^{\beta_{32}\left(\frac{1}{\mathrm{T}_0}-\frac{1}{\mathrm{T}}\right)} \frac{R_{f32}}{R_{f32o}}\right] + c \tag{6}$$

a, *b* and *c* being empirically determined in a preliminary calibration phase, *eqn.* (6) can be solved to determine the temperature from the measurements of the ratios R_{f12} and R_{f32}.

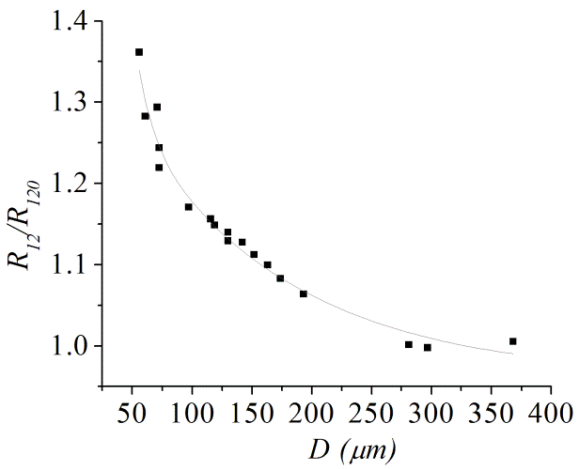

Figure 4. Evolution of the normalized fluorescence ratio as a function of the droplet diameter of calibrated single droplets (from [21]).

3.2 Set-up of the combined 3cLIF-PDA technique

The optical arrangement for combined 3cLIF-PDA measurements is illustrated in Figure 5 (top view). The objective is to combine a phase Doppler system with the 3c-LIF thermometry in order to derive the droplet temperature per size class before and after the impact.

3.2.1. PDA measurements

A phase Doppler analyzer manufactured by Dantec-Dynamics® is used to measure the droplet diameter and the vertical component of the droplet velocity *w* (along the *Z*-axis). It includes a classic reception optical device (label (10) in Figure 1) and a P80 signal processor. The laser excitation volume is generated by a LDA transmitter probe (Dantec-dynamics Fiber-Flow® probe; label (9)) and by using the green line (λ = 514.5 nm) of the same argon ion laser for fluorescence excitation. Unfortunately, it was not possible to measure the horizontal component *v* of the velocity (along the radial coordinate *r*). In fact, the available blue line of the laser is located within the absorption spectrum of the fluorescent tracer. Therefore, the emission spectrum would be affected and the current 3cLIF technique would not be longer valid. The focal front lens of the transmitter probe is 1200 mm while the focal length of the receiver is 500 mm, leading to a maximum detectable droplet size of 327 µm. The PDA measurement volume is defined as the intersection of the illuminated volume with the projection of a slit aperture (width of 120 µm) included in the PDA receiver. Taking into account the magnification and the effect of the off-axis angle, the measurement volume is approximated by a cylinder that is truncated obliquely, having a diameter of 220 µm.

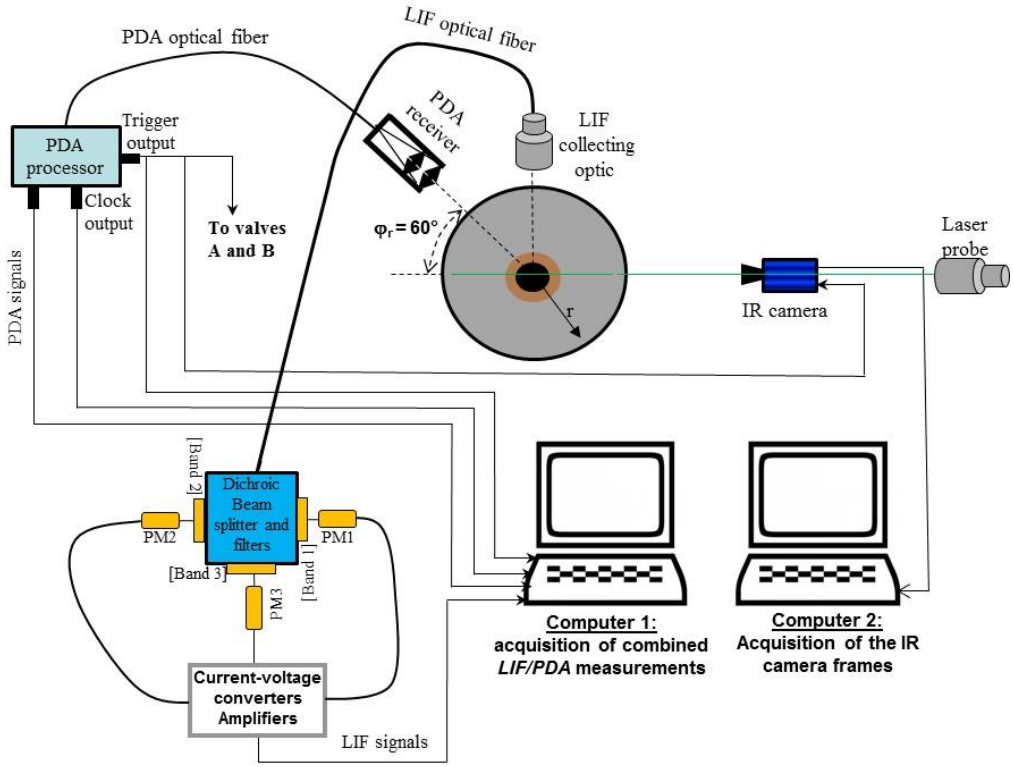

Figure 5: Top view of the arrangement of 3cLIF-PDA devices, IR thermography devices and principle of their synchronization.

Due to the presence of the experimental chamber, the receiver is elevated with an angle of 45° from the solid surface. As a consequence, since the receiver is not in the plane parallel to the fringes system generated within the excitation volume, the elevation angles of the three photomultipliers are modified. It is then necessary to revise the calculation of both phase factors in order to correct the diameter derivations [28]. The PDA is operated in the first refraction mode with an off-axis angle of 60° (Figure 5). Otherwise, due to the high liquid flow rates injected, the impingement on the surface is characterized by a great amount of expelled droplets causing wide optical signal disturbance if the measurement volume is too close to the surface. As a consequence, all measurements undertaken in this paper are obtained at a distance of 15 mm above the surface, ensuring a suitable quality of the optical signal.

3.2.2. 3cLIF measurements and data processing

To perform 3cLIF measurements, the fluorescence is induced by using the previous PDA detection volume. The fluorescence signal is collected at right angle by means of an achromatic doublet (focal front lens of 500 mm) and coupled with an optical fiber having a core diameter of 70 µm. In this case, the measurement volume is the intersection between the laser illuminated volume with the projected image of the optical fiber core. Knowing the magnification of the achromatic doublet, the LIF measurement volume is also a cylinder having a diameter of 350 µm. The collected signal is then high-pass filtered (Chroma®, HQ522LP) in order to remove the light scattered by the droplets at the laser wavelength. The remaining fluorescence signal is split into the three spectral bands of interest by means of a set of dichroics and interference filters (Figure 5). The fluorescence is detected by means of three photomultiplier tubes and digitalized with an acquisition board (computer (1) in Figure 5). The detection of the LIF signal emitted by the droplet transits in the probe volume is achieved by means a threshold that is fixed significantly above the noise level of the channels of detection (signal conditioners and photomultiplier tubes). If a sequence has more than ten consecutive samples above this threshold, it is considered coming from droplets. The fluorescence ratio R_{fij} (i or j denoting the detection channel 1, 2 or 3) is then calculated as follows:

$$R_{fij} = \frac{\sum_{k=1}^{n} I_{fi,k-N_i}}{\sum_{k=1}^{n} I_{fj,k-N_j}} \tag{7}$$

where $I_{fi,k}$ and $I_{fj,k}$ are respectively the fluorescence intensities integrated on the kth droplet crossing the detection volume. n is the number of droplets detected during the acquisition period. N_i and N_j are the average dark noise values on the corresponding detection channels.

3.2.3. Combined LIF-PDA measurements

Combining both PDA and 3cLIF devices consists in synchronizing the acquisition of the signal incoming from both devices and matching them. To attain this goal, the trigger output of the PDA processor is used to drive the LIF acquisition board and the external clock of the PDA processor timed at 5 MHz is used to sample the LIF signal, so that both devices are operated with the same time origin and the same time base. Therefore, the combined 3cLIF-PDA system provides two synchronized data files, one corresponding to the normal droplet velocity and droplet diameter measured by the PDA and the other one to the fluorescence intensity integrated on the droplet transit in the common detection volume for the three spectral bands of detection. The common detection volume is the intersection of both PDA and 3cLIF measurement volumes. Due to the large size of the LIF detection volume, the common detection volume is then limited by the PDA detection volume. The droplets detected simultaneously by PDA and 3cLIF are identified on the basis of their arrival time and their transit time. Then, a fixed number of droplet size classes are defined and the fluorescence intensities on each detection channel are averaged following *eqn*. (7), for each of the droplet size classes. As a result, an average fluorescence ratio can be associated to a given droplet size class characterized by an average diameter D_c. Moreover, by using the sign of the normal velocity component w, it is possible to discriminate the droplets that are coming onto the heated surface from the droplets that rebound or splash on the surface. Consequently, in the following, subscripts b and a will denote velocity, diameter or temperature before and after impact respectively.

3.3 Wall heat flux measurements

The heat flux density removed by the spray is estimated by infrared thermography (IRT). An infrared camera (Cedip® Jade III; spatial resolution of 320 × 240 pixels), equipped with a narrow-bandwidth spectral filter ([3.97 µm-4.01 µm]), is used in order to measure the temperature field of the

rear face of the solid wall (opposite to the spray impact). An analytic inverse heat conduction model within the disk is used to estimate the heat flux extracted by the spray on the front face [11; 29]. An angular averaging of the measured temperature is computed to estimate the heat flux extracted by the liquid $\varphi_w(r, t)$ as a function of the radial position r. Previously, the calibration of the camera is performed by heating the disk up to 800°C and by recording simultaneously the infrared signal and the temperature with the use of a K-thermocouple inserted just 2 mm below the front face of the disk, while the disk cools naturally. Due to the spectral range of the sensor, the sensibility of the camera at low temperature is weak and the lowest measurable by IRT is about 100°C. Since the cooling phase has a typical duration of about 30 s, the number of frames per run is about 2000, which are stored on the computer 2 (Figure 5). Thus, the sampling frequency was adjusted at about 60 Hz. Due to the presence of the insulating holder that maintained the nickel disk, the disk area visualized by the IR camera was truncated. Thus, only a limited part if the surface can be investigated, up to $r/R = 0.8$.

3.4 Acquisition procedure and data post-processing

As mentioned previously, each experiment begins by heating the disk up to a surface temperature of about 800°C (controlled by the IR camera). Then, the cooling process is started and both IRT and combined 3cLIF-PDA techniques are synchronized to analyze properly the cooling phase. As for combined 3cLIF-PDA, the trigger output of the PDA processor is also used to drive the IR camera as well as the switching of both electro-valves that control the spray flows (Figure 5). This procedure allows monitoring simultaneously the heat flux, the velocity, the diameter and the temperature of the droplets before and after impact. The acquisition is stopped when the surface temperature reaches roughly the ambient temperature, but the exploitation is limited for temperatures higher than 100°C.

The first cooling experiments that were conducted show that the vapor generated during the rewetting regime is deposited on the surface of the front lens of both 3cLIF and PDA receivers, which causes major disturbances due to the dramatic decrease of the quality of the optical signal detection. Therefore, the analysis of combined 3cLIF-PDA and IRT data is limited to the Leidenfrost regime duration, denoted by Δt_{Leid}, the vapor generation being very limited.

Table 2 summaries the quantities derived from the combined 3cLIF-PDA and IRT measurements that will be used for the analysis of the heat and mass transfers involved in the Leidenfrot regime. In a recent work [30], it was observed that droplet properties before and after impact were independent on the surface temperature during the Leidenfrost regime. Thereby, all diameters and velocities presented in Table 2 are quantities averaged during Δt_{Leid}, *i.e.* the Leidenfrost regime. However, the droplet properties may depend on the position above the disk (*i.e.* along Z and r axis). In addition, two kinds of incident normal Weber numbers before and after impact can be deduced:

i. the normal Weber number We_n based on the diameter for a given diameter class D_c and the normal velocity w_d of the corresponding diameter class:

$$We_n = \frac{\rho w_d^2 D_c}{\sigma} \tag{8}$$

The relationship between D_c and w_d is deduced from the normal velocity-droplet size correlation obtained with the PDA measurements.

ii. the mean normal Weber number $\widehat{We_n}$ based on both the arithmetic normal velocity $\widehat{w_d}$ and diameter D_{10}:

$$\widehat{We}_n = \frac{\rho \widehat{w}_d^2 D_{10}}{\sigma} \tag{9}$$

From IRT technique, it is possible to measure the heat flux density φ_w as well as the surface temperature T_w as a function of the time at any coordinate r. From combined 3LIF-PDA measurements,

two kinds of local temperatures are derived: a local temperature per size class $\tilde{T}$ and a mean temperature $\tilde{T}_m$ defined as following [24]:

$$\tilde{T}_m = \frac{\sum_{p=1}^{N_c} D_p^{2.8} N_\mathrm{p} \tilde{T}_p}{\sum_{p=1}^{N} D_p^{2.8} N_\mathrm{p}} \tag{10}$$

where p is the droplet size class index, N_c the number of size classes, N_p the number of droplets per size class and $\tilde{T}_p$ the temperature corresponding to the pth class.

A preliminary 3cLIF-PDA measurements is conducted in order to determine both the reference and the three parameters a, b and c (*eqn.* (5)) at Z = 45 mm above the disk (not heated) with one spray. A thermocouple is used to measure the reference temperature T_0 at the injection. By plotting both normalized ratios (R_{f12}/R_{f120} and R_{f32}/R_{f320}) per droplet size class (10 classes are taken), parameters a, b and c are deduced.

For the cooling experiments, both temperatures ($\tilde{T}$ and $\tilde{T}_m$) are calculated from all droplets that are commonly detected by both PDA and LIF systems during the Leidenfrost regime. Similarly as for the diameter and velocity, one can assume that the droplet temperature is also independent on the surface temperature during the Leidenfrost regime. Beside, this assumption has been well verified in the case of single droplets impinging on a heated wall for Leidenfrost conditions [12]. A very limited effect on the droplet temperature after impact has been noticed when the surface temperature varies. Obviously, both temperature per size class and mean temperature may change according the spatial location (*i.e.* along Z and r axis).

Table 2: Summary of the post-processed quantities deduced from the three diagnostics and used for the heat and mass transfer investigations; all LIF and PDA quantities are time-averaged during the Leidenfrost regime.

Phase Doppler system	Droplet class diameter before D_b and after D_a impact	Mean diameter before D_{10b} and after D_{10a} impact	Normal velocity per droplet size class before w_{db} and after w_{da} impact	Mean normal velocity before $\widehat{w_{db}}$ and after impact $\widehat{w_{da}}$
	Unity: μm Variables: r, Z	Unity: μm Variables: r, Z	Unity: m/s Variables: r, Z	Unity: m/s Variables: r, Z
Infrared thermometry + inverse conduction model	Heat flux density φ_w		Surface temperature T_w	
	Unity: W/m^2 Variables: r, t		Unity: °C Variables: r, t	
Combined 3cLIF-PDA	Temperature per droplet size class before $\tilde{T}_b$ and $\tilde{T}_a$ after impact		Mean droplet temperature before $\tilde{T}_{mb}$ and after impact $\tilde{T}_{ma}$	
	Unity: °C Variables: r, Z		Unity: °C Variables: r, Z	

3.5 Uncertainties

The global error of the combined 3cLIF-PDA technique depend on both errors on LIF and PDA measurements. The accuracy of the LIF technique is linked to the number of samples used to derive the fluorescence ratio and the droplet diameter, which is related to the amount of available signal intensity. In the previous studies devoted to the use of this technique [23; 25], the duration of the acquisition was adjusted in order to obtain a stochastic error on the mean value of the fluorescence ratio inferior to 0.5 %, leading to an error of about ± 5°C. Increasing the number of diameter classes requires obtaining a great number of detected droplets and then increasing the duration of the acquisition. For instance, a reliable acquisition sequence requires the collection of at least 500 droplets for a diameter class of 100 µm and 1000 droplets for a diameter class of 20 µm [23]. In

the present study, the short duration of the Leidenfrost regime doesn't allow collecting a sufficient number of droplets. Consequently, only three size classes D_c are used: D_c = 37.5, 102.5 and 167.5 µm. Typically, with our conducted experiments, the number of averaged droplets on each of the three classes is about 850, 550 and 100. As it will be show below, these low numbers leads obtaining scattered temperature results. Certainly, this difficulty represents a main drawback of the combined 3cLIF-PDA technique.

The evaluation of the error magnitude is generally difficult to determine for quantities obtained with the PDA system. In such a device, the dynamic of the droplet size and velocity is fixed by the optical configuration (laser wavelength of both beams and focal length of lenses for both emitting and receiving probes), the photomultiplier high voltage and the electro-optical gain. However, without changing these parameters, it is possible to estimate a relative error by performing repetitive measurements in a same position in the spray. Presently, this relative error is in the worst case about 10% for both mean velocity and mean diameter.

The accuracy of the IRT measurements results from the inverse heat transfer algorithm and cannot be directly assessed, even if the error for each of the parameters included in the model (thermophysical properties and temperature measurements) is known, another bias can be introduced if the heat conduction model is far from reality. The estimation of the bias in the heat flux must be done using simulated temperature obtained after a direct simulation of the set of equation [11]. The obtained temperature field, if all the initial parameters (boundary conditions, thermophysical properties) are known, is used as input data of the inverse model in order to compare the results of the inversion procedure with the input data (*i.e.* boundary conditions for direct simulations). From these tests, the uncertainties on the estimation of the heat flux and temperature are less than 10%.

4. Results and discussion

4.1 Experimental protocol

As combined 3cLIF-PDA technique is a pointwise measurement, a 3D traverse system (label (8) in Figure 1) is used to move the measurement volume along the *Z* and *r* axis. It means that, for one given spray, the cooling sequence must be repeated several times in order to map all the spray volume. For a given spray, although the spray is not changed, the heat flux density is measured at each experiment, *i.e.* for each *(Z, r)* locations. Nevertheless, the repeatability of the cooling sequence is well verified and only one IRT measurement for each spray is used for the following analysis.

All present measurements are performed at three radial positions above the surface (r/R = 0, 0.5 and 0.8) for the three investigated sprays. It represents a set of 9 experimental tests.

On the other side, as the total volume of coolant is limited, the repetition of the cooling experiments leads to an increase of the water temperature at the injection. Therefore, the acquisitions of data are not performed until the temperature stabilizes, typically at a value of about 35°C.

4.2 Investigation of the droplets heating using combined 3cLIF-PDA.

Figure 6 shows typical droplet temperature results obtained for the three sprays. It represents the droplets heating (*ie* droplet temperature after impact minus droplet temperature before impact) for the class diameter of 37.5 µm (a), 102.5 µm (b) and 167.5 µm (c). It appears that the heating increases with the droplet diameter class. But it seems that for each size classes the heating is similar regardless the spray. Moreover, except for the smallest size class where a slight decrease of the heating may be observed, the heating seems also doesn't depend on the radial position. In Figure 7, the droplet heating along the *r*-axis is compared for the three size classes for the spray 1 (a), the spray (2) and the spray (3). Again, one can observed that the droplet heating increases with the size class and that no effect of the kind of spray is noticed.

On the contrary, the study of the mean droplet heating $\Delta\tilde{T}_m$ reveals a dependence of the spray properties (Figure 8). The mean heating corresponds to the increase of the mean droplet temperature during the impact whatever the droplet size: $\Delta\tilde{T}_m = \tilde{T}_{ma} - \tilde{T}_{mb}$. Figure 8 shows that spray 1 leads to higher mean droplet heating compared the two others sprays. By comparing with Figure 3, one can conclude that the mean droplet heating is strongly correlated with the mean normal Weber number We_{nb} (*eqn. (9)*). Indeed, the analysis of the droplet heating is generally performed by using two relevant parameters before impact as the Weber number or the Mundo number K ($K = WeOh^{-0.4}$, Oh being the Ohnesorge number defined as $Oh = \mu/(\rho D_c \sigma)^{1/2}$). These parameters depend on the droplet size class. Unfortunately, in this study, the direct use of the droplet size class before impact for analyze the heating is not straightforward. Indeed, the present methodology combining LIF with PDA doesn't allow distinguishing the origin of a droplet detected after impact. Within a given size class after impact, the corresponding droplets may be the result of rebounds or from the disintegrations of incoming droplets into secondary droplets (splashing regime). Consequently, it is then difficult to interpret the droplet temperature per size class after impact by attributing a relevant incident Weber number.

According [4; 31], knowing the Mundo number of an incoming droplet and the wall temperature T_w, it is possible to determine the impact regime that may occur on the heated surface (Figure 9), where T^* is a dimensionless temperature defined as:

$$T^* = \frac{T_w - T_{sat}}{T_{Leid} - T_{sat}} \tag{11}$$

In the present study, as only the Leidenfrost regime is considered (*ie* $T_w > T_{Leid}$), T^* is always greater than 1. Here, three droplet size classes are taken for each of the 9 experimental tests, representing 27 cases. Thus, by computing the Mundo number K for these 27 cases, it appears that only four cases lead to $log\ (K) < 2.5$ (rebound regime). As a result, one can assume that the splashing is the main interaction regime and thus, one can interpret the droplet heating as a function of the normal incoming Weber number We_{nb}.

In Figure 10, the droplet heating ΔT is plotted as a function of the normal Weber number We_{nb} for the 27 investigated cases. The heating is obtained for each spray by making the difference between the droplet temperature per size class after impact T_a and the droplet temperature per size class before impact T_b.

The four cases within the blue circle corresponds to the rebound regime. Up to We_{nb}= 500, the droplet heating increases with We_{nb} and for higher values, the data describe a plateau. Dunand et al. [12] and Castanet et al. [32], with single calibrated droplets, have observed a similar behavior. The increase of the droplet temperature being attributed to an increase of the spreading rate of the droplet on the surface favoring the heat transfer between the droplet and the surface. The plateau is interpreted as the maximum spreading rate, reducing the heat transfers.

However, a certain scattering of the results is observed, mainly due to the too lower number of droplets within each size class as mentioned in the previous section 3.5. To reduce this drawback, one can plotted the mean heating as a function of the mean normal Weber number We_{nb} where results are less scattered (Figure 11).

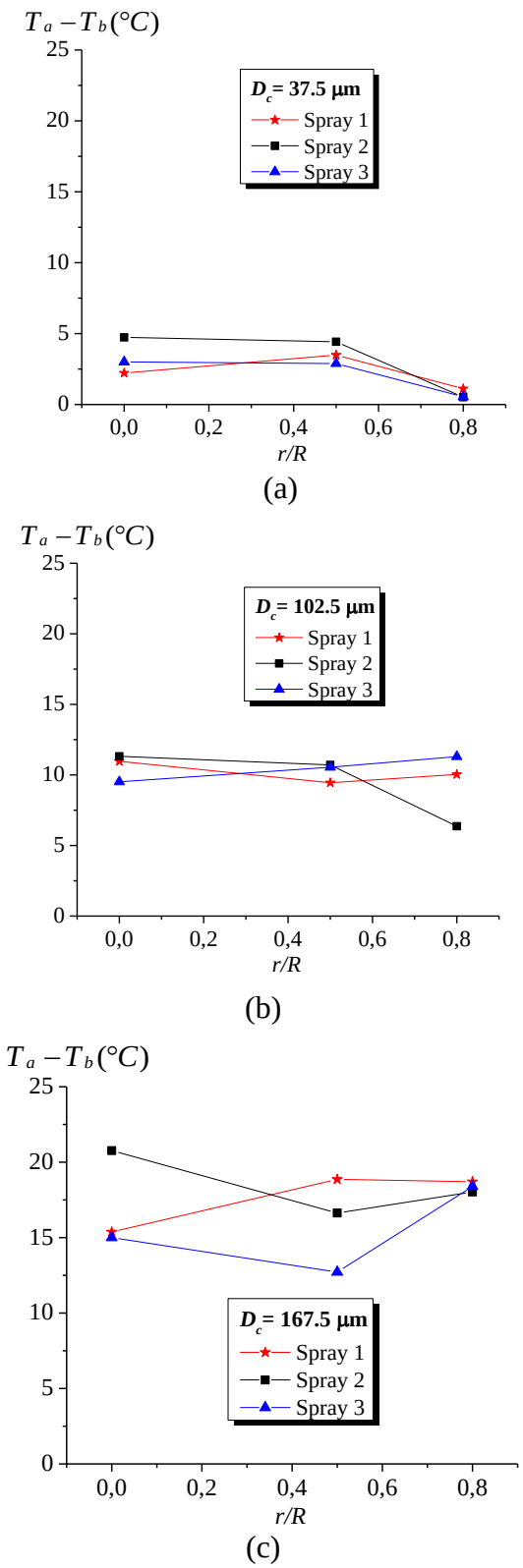

Figure 6. Evolution of the droplet temperature for the three sprays along the *r*-axis and for the three diameter classes D_c: 37.5 µm (a), 102.5 µm (b) and 167.5 µm (c).

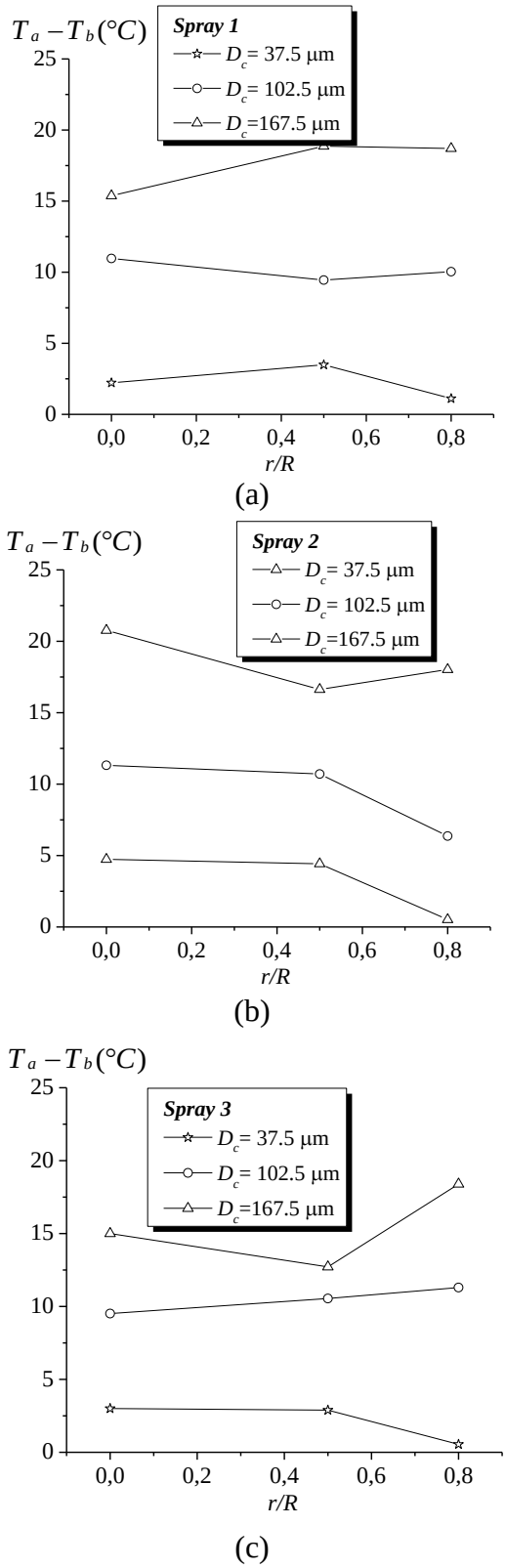

Figure 7. Evolution of the droplet temperature for the three diameter classes D_c along the *r*-axis and for the three sprays: sprays 1 (a), spray 2 (b) and spray 3 (c).

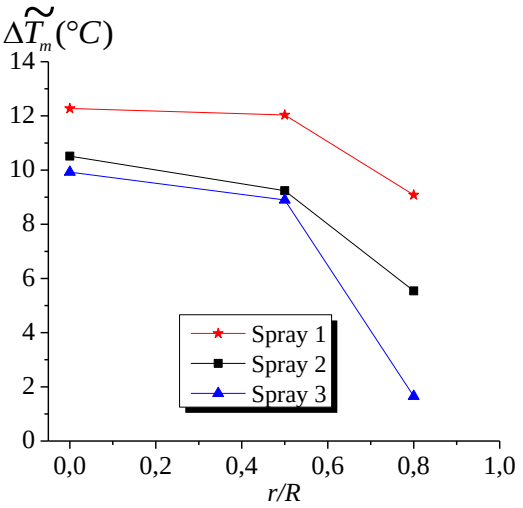

Figure 8. Evolution of the mean droplet heating along the *r*-axis for the three sprays.

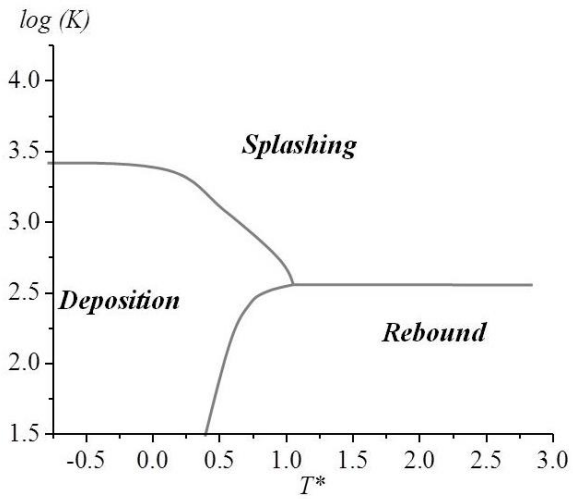

Figure 9. K-T^* diagram representing the boundaries between the different impact regimes according to dimensionless surface temperature and Mundo number (Cossali et al., 2005 and Dewitte et al., 2005).

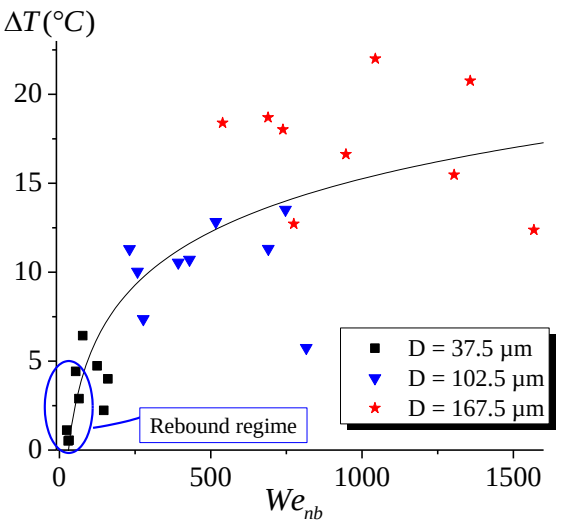

Figure 10. Heating of the droplets as a function of the incident normal Weber number.

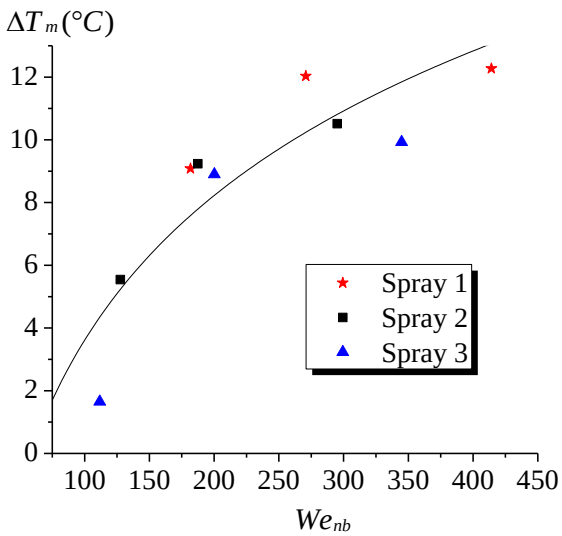

Figure 11. Mean heating of the droplets as a function of the mean incident normal Weber number.

4.3 Heat and mass transfers balance

In this section, the energy balance resulting from heat and mass transfers that occur during the cooling phase was investigated by using the IRT and combined 3cLIF-PDA. One of the objective is to estimate the mass of the evaporated liquid during the Leidenfrost regime. This study is performed with the set of 9 experimental tests: the three positions and the three sprays.

4.3.1. Energy balance of a droplet /wall interaction

The energy balance is undertaken for an incoming single droplet that impacts the surface during the Leidenfrost regime. This balance is assumed valid whatever the impingement regime. The dif-

ferent heat fluxes of this balance are illustrated in Figure 12. The droplet before impact has an initial mass m and a temperature T_b. After impact, this droplet temperature rises to T_a and the mass becomes $m - m_e$, where m_e is the evaporated liquid mass. In the particular case of the Leidenfrost regime, a vapor film at the temperature T_v is present above the surface at the temperature T_w. Another component in this balance is the spray flow that induces an air flow, tangentially to the disk surface, at a velocity v_{air}.

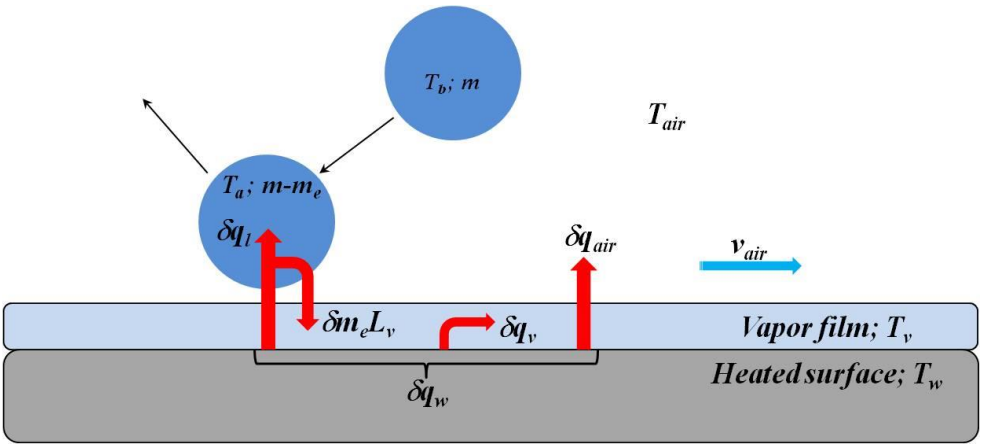

Figure 12. Energy balance established for a single droplet impinging on a heated wall above the Leidenfrost temperature.

Thereby, by neglecting the surface radiative emission, the total energy extracted from the surface can be written as the sum of four main contributions:

i. The sensible heat gained by the droplet δq_l
ii. The phase change heat $\delta_{me} L_v$
iii. The heat drained by the vapor film between the droplet and the wall δ_{qv}
iv. The heat removed by the horizontal entrained airflow δq_{air}

As the surface temperature T_w varies in time, the energy balance is written at each time step δt of the cooling sequence. In fact, the frequency of 60 Hz for the IR frames acquisition is taken equal of the time step (δt = 0.016 s). Moreover, the balance energy is written per unit surface (*i.e.* in J/m²). Therefore, the instantaneous energy balance density is:

$$\delta q_w(r,\delta t) = \delta q_l(r,\delta t) + \delta m_e(r,\delta t) L_v + \delta q_v(r,\delta t) + \delta q_{air}(r) \tag{12}$$

where δq_w is deduced from the IRT:

$$\delta q_w(r,\delta t) = \varphi_w(r,t)\delta t \tag{13}$$

The expression (12) shows a limit of the abilities of these experiments. Indeed, the heat flux density measured by IRT corresponds to the heat flux extracted from all the droplets impinging onto the surface regardless their sizes and the impact regime. Thus, only the mean droplet temperature at a given radius position can be used in *eqn* (12). As a result, the sensible heat density carried by the liquid, at a given radial r position, may be written as:

$$\delta q_l(r,\delta t) = c_{pl}\left[\delta m(r) - \delta m_e(r,\delta t)\right]\left[T_{ma}(r) - T_{mb}(r)\right] + c_{pl}\delta m_e(r,\delta t)\left[T_{sat} - T_{mb}(r)\right] \tag{14}$$

In this expression, δm is the liquid mass density (in kg/m²) impinging the surface during the time interval δt. It can be deduced by using the liquid mass flux distribution G (Figure 2): $\delta m(r) = G(r)\delta t$. Obviously, it is assumed that the quantity of liquid impinging the surface at a given position r is constant over time. The term δm_e is the evaporated liquid mass density (in kg/m²),

which depends on both time and radial coordinate. T_{ma} and T_{mb} are respectively the mean droplet temperatures after and before impact measured with combined 3cLIF-PDA measurements. It is assumed that the droplet temperature just after impact is roughly the same as at 15 mm above the surface.

Then, the heat density drained by the vapor is expressed by:

$$\delta q_v(r,\delta t) = \delta m_e(r,\delta t) c_{pv}(T_v(r,\delta t) - T_{sat}) \tag{15}$$

The vapor temperature T_v is unknown and not measured. To that purpose, the film temperature is taken into consideration:

$$T_v(r,\delta t) \approx T_{film}(r,\delta t) = \frac{T_w(r,\delta t) + T_{sat}}{2} \tag{16}$$

Due to the dependence on T_w, it appears that T_v depends on both variables t and r.

The term δq_{air} is the heat density removed by forced convection due the entrained airflow along the surface. It can be written as

$$\delta q_{air}(r,\delta t) = h_{air}(r)\left[T_w(r,\delta t) - T_{air}\right]\delta t \tag{17}$$

where h_{air} is the convection heat transfer coefficient and T_{air} the ambient temperature taken far away from the surface. In order to estimate h_{air}, the Nusselt correlation for a turbulent airflow along a flat plate at a given position r along the plate is considered:

$$Nu(r) = 0.029\,\mathrm{Re}_r^{4/5}\,\mathrm{Pr}^{1/3} = \frac{h_{air} r}{k_{air}} \tag{18}$$

Where Re_r is the Reynolds number at the radius r ($Re_r = v_{air}.r/\upsilon_{air}$), Pr and k_{air} are the Prandtl number and the thermal conductivity of air respectively taken at T_{film}. The calculation of the Reynolds number requires the knowledge of the velocity v_{air} along the r-axis. The entrained airflow velocity can be assumed equal to the velocity of the smallest droplets, due to their low stokes. In that way, the horizontal component of the velocity/droplet size correlation obtained from PDA measurements could be used. However, in the present work, the radial velocity component is not measured (reasons explained in section 3.2). Then, the results obtained in a previous study conducted in same operating conditions (same nozzles and impinging conditions) are used [26]. Figure 13 presents an example of the correlation of the droplet size and the radial velocity of the incoming droplets for the spray 1 (measurement at $r = 0$ and $Z = 15$ mm). In this example, the radial velocity of the lowest diameter droplets is used as the airflow velocity, which is about 0.9 m/s (red dash line). As it will be discussed in the last section, even by multiplying the velocity with a factor of two, the contribution of the air to cool the disk remains marginal. This procedure is applied for the three sprays and three r/R positions.

Finally, introducing the Jakob number, $Ja = c_{pv}(T_{film} - T_{sat})/L_v$, the instantaneous mass density of the evaporated liquid during the Leidenfrost regime at a given time interval δt and a r position can be expressed by:

$$\delta m_e(r,\delta t) = \frac{\varphi_W(r,t) - h_{air}(r)\left[T_W(r,\delta t) - T_{sat}\right] - G(r)c_{pl}\left[Tma(r) - Tmb(r)\right]}{L_V\left[1 + Ja(r,\delta t)\right] + c_{pl}\left[T_{sat}(r) - Tma(r)\right]}\delta t \tag{19}$$

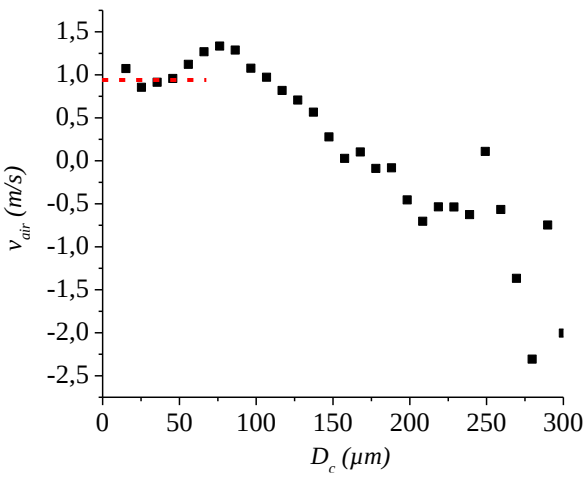

Figure 13. Example of radial velocity component/droplet size correlation for the incoming droplets of the spray 1 measured at r = 0 and Z = 15 mm.

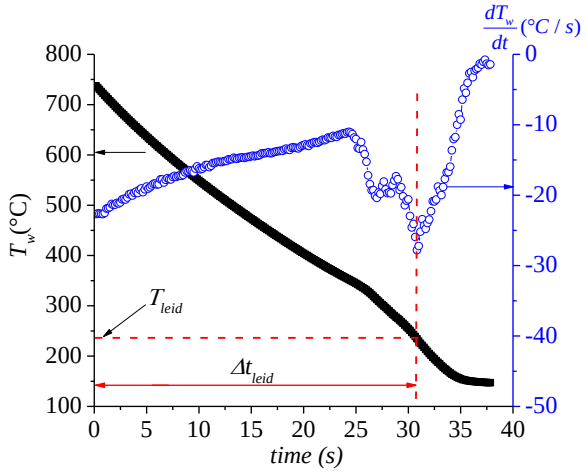

Figure 14. Evolution of the surface temperature and its time derivative during the cooling for the spray 1 at r/R = 0.

In summary, the calculation of δm_e (*eqn* (19)) requires to knows:

- the heat flux extracted by the droplets from the wall φ_w from IRT measurements,
- the heat transfer coefficient h_{air} deduced from *eqn* (18) and from PDA measurements,
- the surface temperature T_w from IRT measurements,
- the liquid mass flux G from Figure 2,
- both mean droplet temperature T_{ma} and T_{mb} from combined 3cLIF-PDA measurements,

However, the use of *eqn* (19) requires firstly to determine the duration of the Leidenfrost regime Δt_{Leid}, *i.e.* when the surface temperature is above the Leidenfrost temperature T_{Leid}. From IRT measurements, the Leidenfrost temperature can be easily accessible by plotting the surface temperature as a function of time. For instance, Figure 14 shows an example of temperature evolution in the case of spray 1 at r/R = 0 and its time derivative. The time corresponding to the end of the Leidenfrost regime occurs when the time derivative experiences a minimum.

4.3.2. Investigation of the evaporated liquid mass

Figure 15 depicts typical evolution of the relative mass of evaporated liquid ($\delta m_e / \delta m$) as a function of the cooling time for the three sprays plotted at r/R = 0 (a) and r/R = 0.8 (b). It appears that the loss of liquid mass is on the order of several percent. At the center (r/R = 0), higher liquid evaporated rates is reached with spray 2 whereas it is similar for the two others. At the edge of the disk (r/R = 0.8), spray 2 and 3 describe similar evolution and lead to higher amount of vapor compared to spray 1. In addition, the three curves at r/R = 0.8 describe higher slopes than in the center meaning that higher amount of vapor is produced toward the edge of the disk. This phenomenon is due to the draining of the vapor toward the edge promoting the vaporization of the liquid or reducing the phenomenon of vapor saturation.

Now, the goal is to correlate the liquid vaporization with spray properties as well as droplet heating. For that purpose, Figure 8 and 15 are firstly compared. It appears globally that higher droplet heating disadvantage vapor generation. Indeed, without regarding the case of spray 3, spray 1 leads to the lowest vaporization and presents the highest droplets heating. Next, one can compared both Figures 2 and 3 (evolution of the liquid mass flux and normal Weber number respectively) with Figure 15. One can observe that higher normal Weber number tends decreasing the vapor generation. On the other hand, no correlation with the liquid mass flux G (Figure 2) can be clearly es-

tablished. In fact, this parameter is usually strongly correlated with the global heat flux extracted by the spray from the hot surface. It is often observed that the heat flux increases with the liquid mass flux [5; 6; 10; 26].

The vapor generation dependence with the normal Weber number and the droplet heating is then verified for all the 9 experimental tests (*ie* the three radial positions and the three sprays) and over the Leidenfrost regime (*i.e.* from $t = 0$ up to $t = \Delta t_{Leid}$). More precisely, δm_e was cumulated over all the time intervals i (i varying between from 1 up to n, n being the number of points describing the cooling) according to:

$$m_e(r) = \sum_{i=1}^{n}\left(\delta m_{e_i}(r,\delta t)\delta t\right) = \delta t\left(\sum_{i=1}^{n}\delta m_{e_i}(r,\delta t)\right) \tag{24}$$

In Figure 16 is depicted the evolution of m_e (relatively to the impinging liquid mass $m(r)$) as a function of the mean droplet heating ΔT_m. The distinction between of the three sprays is maintained. One can observe an overall decreasing of the vapor generation with the mean droplet heating. Similarly, the relative loss of liquid m_e decreases also with the mean normal Weber number We_{nb} (Figure 17). At the same time, these both Figures are in well agreement with Figure 11: a decrease of the normal Weber number leads to a decrease of the droplet heating. Furthermore, Figures 17 and 18 shows that lower liquid vaporization is globally obtained with the spray 1, confirming then the previous findings (Figure 15).

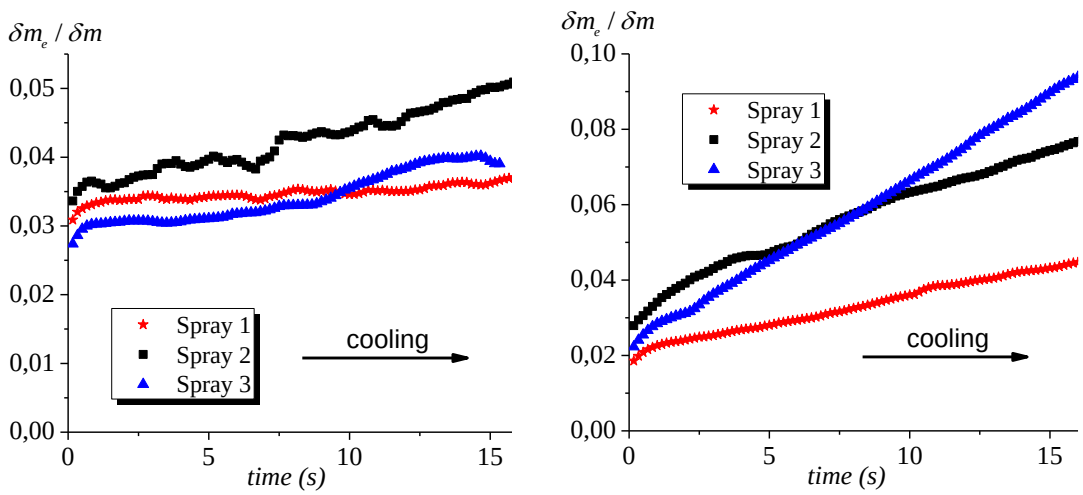

(a) (b)

Figure 15. Evolution of the relative mass of vapor production as a function of time during the Leidenfrost regime for the three sprays plotted at $r/R = 0$ (a) and $r/R = 0.8$ (b).

After all, the total mass of vapor produced above the surface is compared for the three sprays. The vapor density $\delta_{me}(r, \delta t)$ is obtained by integrating *eqn.* (19) over the surface as following:

$$\overline{\delta m_e}(\delta t) = \left(\frac{1}{\pi R^2}\int_0^R \delta_{me}(r,\delta t)2\pi r dr\right)\delta t \tag{20}$$

This integration is performed with the help of the three investigated positions r/R for each sprays. Figure 18 displays the time evolution of the relative space-averaged vapor density $\overline{\delta m_e} / \overline{\delta m}$ for the three sprays. $\overline{\delta_m}$ is the total of liquid mass impinging the surface at each time interval δt and is given by:

$$\overline{\delta m} = \left(\frac{1}{\pi R^2}\int_0^R G\,(r) 2\pi r dr\right)\delta t \tag{21}$$

where G is deduced from Figure 2.

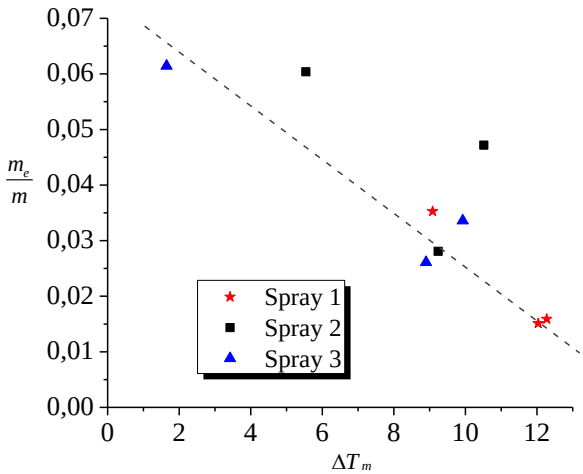

Figure 16. Evolution of the relative loss of mass density integrated during the Leidenfrost regime as a function of the mean droplets heating for the three sprays.

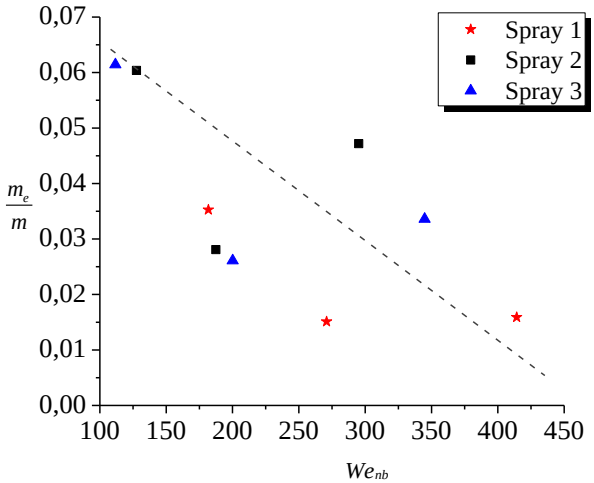

Figure 17. Evolution of the relative loss of mass density integrated during the Leidenfrost regime as a function of the incident mean normal Weber number for the three sprays.

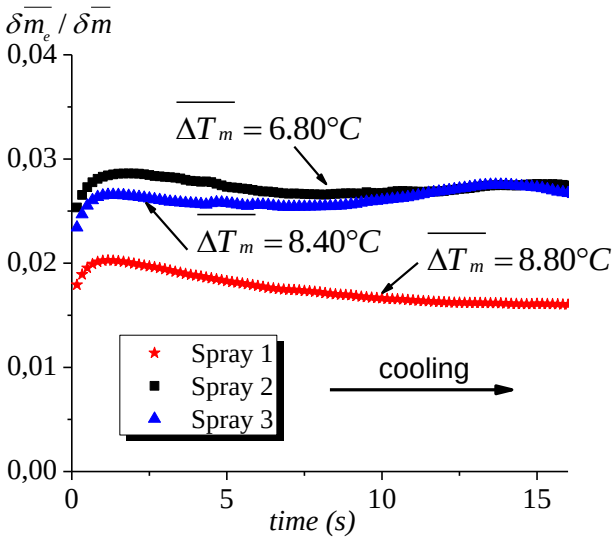

Figure 18. Evolution of the relative total mass of vapor production above the surface as a function of time during the Leidenfrost regime for the three sprays.

Figure 18 shows clearly that spray 2 and 3 produce higher amount vapor than spray 1. Their productions are about twice of spray 1. This observation is again correlated with the droplet heating. In Figure 18, the mean surface droplet heating $\overline{\Delta T_m}$ (mean droplet heating integrated over the disk surface) is marked for the corresponding three sprays. As expected, spray 1 leading to the highest droplet heating produces low amount of vapor.

4.3.3. Comparison of the heat flux contributions

Knowing the instantaneous mass density of evaporated liquid from *eqn.* (19), it is then possible to compare the four heat contributions during the cooling of the disk. These contributions are compared for the spray 1 above the entire surface at each time step and are derived according the following expressions:

i. The space-averaged sensible heat gained by the droplet:

$$\overline{\delta q_l}(\delta t) = \left(\frac{1}{\pi R^2}\int_0^R \delta q_l\,(r,\delta t) 2\pi r dr\right)\delta t \tag{22}$$

ii. The space-averaged phase change heat:

$$\overline{h_v}(\delta t) = \left(\frac{1}{\pi R^2}\int_0^R \delta m_e\,(r,\delta t) L_v 2\pi r dr\right)\delta t \tag{23}$$

iii. The space-averaged heat drained by the vapor film

$$\overline{\delta q_v}(\delta t) = \left(\frac{1}{\pi R^2}\int_0^R \delta q_v\,(r,\delta t) L_v 2\pi r dr\right)\delta t \tag{24}$$

iv. The heat removed by the horizontal entrained airflow δq_{air}

$$\overline{\delta q_{air}}(\delta t) = \left(\frac{1}{\pi R^2}\int_0^R \delta q_{air}\,(r,\delta t) L_v 2\pi r dr\right)\delta t \tag{25}$$

The evolution of the four heat contributions is shown in Figure 19 for spray 1. The heat extracted from the surface by the spray is also added and is derived as following:

$$\overline{\delta q_w}(\delta t) = \left(\frac{1}{\pi R^2}\int_0^R \varphi_w\,(r,t) 2\pi r dr\right)\delta t = \overline{\varphi_w}(t)\delta t \tag{26}$$

It appears that the cooling of the surface is mainly due to both the heat phase change and sensible heat. Their respective sum corresponds roughly to the total heat extracted $\overline{\delta q_w}(\delta t)$. On the contrary, the effect of the airflow may be neglected while the contribution of the heat drained by the vapor film remains very low.

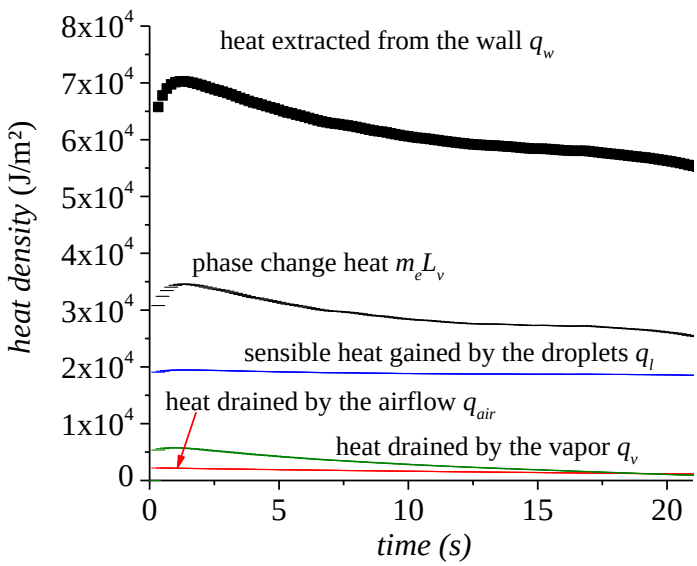

Figure 19. Comparison of the various space-averaged heat contributions for spray 1.

5 Summary and conclusion

This experimental study has mainly demonstrated the abilities of the implementation of combined 3cLIF-PDA with infrared thermography measurements in the case of sprays impinging a heated surface above the Leidenfrost regime at high liquid flow rate. The coupling 3cLIF-PDA device allows obtaining droplet temperature per size class. In parallel, infrared thermography, combined with an inverse heat conduction model, has allowed estimating the heat flux density extracted by the sprays. The synchronization of these three techniques has also allowed monitoring the cooling of the surface as well as the droplet properties (velocity, diameter and temperature) before and after impact. Therefore, an energy balance has been proposed in order to evaluate the mass of liquid that is evaporated during the cooling.

The combination of these three optical diagnostics is tested by investigating the cooling of a nickel disk of 175 mm diameter heated up to a surface temperature of about 800°C. The influence of the normal Weber number is analyzed by using three different full cone sprays and by performing measurements at different locations above the nickel disk. However, the methodology improved in this work presents three drawbacks that limit the interpretation of the obtained results:

1. The short duration of the observed physical phenomenon doesn't allow collecting enough droplets to ensure reliable statistics results. Therefore, the temperature results are scattered.
2. The IRT technique measures the heat flux extracted from the wall by all the droplets whatever their sizes. The influence of the droplet size and their contribution in the energy balance can't be investigated.
3. Due the principle of the coupling 3cLIF-PDA device, the direct correlation of the droplet temperature evolution after impact with the incident normal Weber is not straightforward.

Despite this, by mainly taking into account the splashing regime, 3cLIF-PDA results have allowed highlighting an increase of the droplet temperature with the incident normal Weber number. On the other hand, the study of the energy balance has clearly shown that the mass of evaporated liquid decreases when the incident normal Weber and the droplet heating increases.

Therefore, even if the combination of 3cLIF with PDA and IRT measurements present three limits, the first results are promising and are in well agreement with similar studies conducted with single droplets.

Acknowledgments

The authors would thanks Alain Delconte for his technical support for the set-up of the combined LIF/PDA technique and his help for the corresponding data post-processing.

References

[1] Webb, B.W., Ma, C.F., James, P.H., Thomas, F.I., Single-phase liquid jet impingement heat transfer, Advances in Heat Transfer, (1995) 105-217.
[2] Rioboo R., Tropea C., Marengo M., Outcomes from a drop impact on solid surfaces, Atomization and Sprays, 11 (2001) 155-165.
[3] Sikalo S., Marengo M., Tropea C., Analysis of impact of droplets on horizontal surfaces, Experimental Thermal an Fluid Sciences, 25 (2002) 503-510.
[4] Cossali G.E., Marengo M., Santini M., Single-drop empirical models for spray impact on solid walls: a review, Atomization And Sprays 15 (2005) 699-736.
[5] Bernardin J.D., Mudawar I., Film boiling heat transfer of droplets streams and sprays, International Journal of Heat and Mass Transfer, 40 (11) (1997a) 2579- 2593

[6] Bernardin J.D., Stebbins C.J., Mudawar I., Mapping of impact and heat transfer regimes of water drops impinging on a polished surface, International Journal of Heat and Mass Transfer, 40 (2) (1997b) 247- 267
[7] MudawarI, Valentine W.S., Determination of the local quench curve for sprays-cooled metallic surfaces, Journal of Heat Treating, 7 (1989) 107-121.
[8] Jia W. and Qiu H.H., Experimental investigation of droplet dynamics and heat transfer in spray cooling, Experimental Thermal and Fluids Science, 27 (2003) 829-838.
[9] Chen R.H., Chow L.C., Navedo J.E., Effects of sprays characteristics on critical heat flux in subcooled water sprays cooling, International Journal of Heat and Mass Transfer, 45 (2002) 4033-4043.
[10] Al-Ahmadi H.M., Yao, S.C., Spray cooling of high temperature metals using high mass flux industrial nozzles, Experimental Heat Transfer, 21 (2008) 38-51.
[11] Gradeck M., Ouattara, J.A., Rémy B., Maillet D., Solution of an inverse problem in the hankel space – infrared thermography applied to estimation of a transient cooling flux, Experimental Thermal and Fluids Science, 36 (2012) 56-64.
[12] Dunand, P., Castanet G., Gradeck M., Maillet D., Lemoine F., Energy balance of droplets impinging onto a wall heated above the Leidenfrost temperature, International Journal of Heat and Fluid Flow, 44 (2013), 170-180.
[13] Le Clercq P., Contribution à l'étude expérimentale et théorique des interactions gouttes/paroi, Ph D thesis of Ecole Nationale de l'Aéronautique et de l'Espace, 2000.
[14] Van Beek J., Grosges T., De Giorgi M.G., Global rainbow thermometry assessed by airy and Lonrenz-Mie theories and compared with phase Doppler anemometry, Applied Optics, 42 (2003) 4016-4022.
[15] Vetrano M, Gauthier S, Van Beek J, Boulet P, Buchlin JM Characterization of a non-thermal water spray by global rainbow thermometry, Experiments in Fluids, 50 (2006) 15-22.

[16] Saengkaew S. , Charinpanikul T., Laurent C., Biscos Y., Lavergne G., Gouesbet G., Gréhan G., Processing of individual rainbow signals to study droplets evaporation, Experiments in Fluids, 48 (2010) 111-119.
[17] Vehring R., Schweiger G., Optical determination of the temperature of transparent microparticles, Appl Spectroscopy, 45 (1992) 25-27.
[18] Walfaren GE, Raman spectral studies of the effects on temperature on water structure, Journal of. Chemical Physique, 47 (1967) 114 .
[19] Müller T., Grünefeld G., Beushausen V., High-precision measurements of the temperature of methanol and ethanol droplets using spontaneous Raman scattering, Applied Physics B Lasers Optics, 70 (2010) 155-158.
[20] Lavieille P., Lemoine F., Lebouche M., Evaporating and combusting droplet temperature measurements using two-color laser-induced fluorescence, Experiments in Fluids, 31(2001) 45-55.
[21] Castanet G., Perrin L., Caballina O., Lemoine F. ,Evaporation of closely-spaced interacting droplets arranged in a single row, International Journal of Heat and Mass Transfer, 93 (2015) 788- 802.
[22] Labergue A., Delconte A., Lemoine F., New insight into two-color LIF thermometry applied to temperature measurements of droplets, Experiments in Fluids, 49 (2010) 547-556.
[23] Labergue A., Delconte A., Lemoine F., Study of the droplet size effect coupled with the laser light scattering in sprays for two-color LIF thermometry, Experiments in Fluids, 52 (2012) 1121-1132.
[24] Depredurand V., Delconte A., Lemoine F., Combined PDA and LIF applied to size-temperature correlations measurements in heated sprays, Experiments in Fluids 50 (2011) 561-571.

[25] Labergue A., Delconte A., Lemoine F., Study of the thermal mixing between two non-isothermal sprays using combined three-color LIF thermometry and phase Doppler analyze, Experiments in Fluids, 54 (6), 1-15 (2013).
[26] Labergue A., Gradeck M., Lemoine F., Comparative study of the cooling of a hot temperature surface using sprays and liquid jets, International Journal of Heat and Mass Transfer, 81 (2015) 889-900.
[27] Depredurand V., Miron P., Labergue A., Wolff M., Lemoine F., A temperature-sensitive tracer suitable for two-color laser-induced fluorescence thermometry applied to evaporating fuel droplets, Measurement Science and Technology, 19 (2008) 1-12.
[28] Albrecht H.E., Borys M., Damaschke N., Tropea C., Laser Doplller and phase Doppler measurements techniques, Springer edition, 2003.
[29] Ouattara A., Gradeck M., Maillet D., Remy B., Solution of IHCP estimation of a non uniform source using an inverse heat conduction method based on an analytical solution, Proceedings of Eurotherm, (2008)
[30] Labergue A., Gradeck M., Lemoine F., Experimental investigations of sprays impingement hydrodynamic on a hot surface at high flow rates using phase Doppler analysis and infrared thermography, International Journal of Heat and Mass Transfer, 100 (2016) 65-78.
[31] Dewitte J., Berthoumieu P., Lavergne G., An experimental study of droplet hot wall interactions and a survey of the splashing regime, Proceedings of the 5th International Symposium on Multiphase Flow, (2005).
[32] Castanet G., Lienart T., Lemoine F., Dynamics and temperature of droplets impacting onto a heated wall, International Journal of Heat and Mass Transfer, 52 (2009) 670-679.